wind

MDPI

Article

Limitations of Standard Rain Erosion Tests for Wind Turbine Leading Edge Protection Evaluation

Peter Kinsley [1,*], Sam Porteous [1], Stephen Jones [1], Priyan Subramanian [2], Olga Campo [3] and Kirsten Dyer [1]

[1] Offshore Renewable Energy Catapult, Offshore House, Albert Street, Blyth NE24 1LZ, UK; kirsten.dyer@ore.catapult.org.uk (K.D.)
[2] GE Vernova Hamburg, Millerntorplatz 1, 20359 Hamburg, Germany
[3] GE Vernova Barcelona, Roc Boronat 78, 08005 Barcelona, Spain
* Correspondence: peter.kinsley@ore.catapult.org.uk

Abstract: Blade leading edge erosion (LEE) is a persistent challenge in the wind industry, resulting in reduced aerodynamic efficiency and increased maintenance costs, with an estimated total expense of GBP 1.3M over a 25-year turbine lifetime. To mitigate these effects, leading edge protection (LEP) systems are widely used, but their real-world performance often falls short of predictions based on the standard rain erosion test (RET). This study investigates the limitations of current RET practices, which are designed to accelerate testing but fail to replicate the diverse environmental conditions experienced by wind turbines. Two LEPs with contrasting viscoelastic properties were tested using a novel design of experiments (DoEs) approach. The study explored the droplet impact frequency, combination and sequencing of high or low rainfall intensities, recovery during the inspection period and droplet size effects on erosion behaviour, to uncover significant differences in material performance compared to standard RET conditions. Results, supported by dynamic mechanical analysis (DMA), indicated that the chosen LEPs undergo a transition between elastic and brittle failure modes at a critical impact frequency, influenced by the viscoelastic properties of the material. Importantly, the findings emphasise the need for revised testing protocols across a range of parameters that incorporate realistic environmental conditions to improve the predictability of LEP performance.

Keywords: wind turbine blades; leading edge erosion; leading edge protection; rain erosion testing; environmental characterisation; dynamic mechanical analysis; realistic testing

check for updates

Academic Editor: Giuseppe Failla

Received: 23 November 2024
Revised: 16 January 2025
Accepted: 24 January 2025
Published: 28 January 2025

Citation: Kinsley, P.; Porteous, S.; Jones, S.; Subramanian, P.; Campo, O.; Dyer, K. Limitations of Standard Rain Erosion Tests for Wind Turbine Leading Edge Protection Evaluation. *Wind* **2025**, *5*, 3. https://doi.org/10.3390/wind5010003

Copyright: © 2025 by the authors. Licensee MDPI, Basel, Switzerland. This article is an open access article distributed under the terms and conditions of the Creative Commons Attribution (CC BY) license (https://creativecommons.org/licenses/by/4.0/).

1. Introduction

Blade leading edge erosion (LEE) remains a critical issue for the wind industry [1,2]. The predominant universal mechanism for LEE is in the form of rain precipitation, which impacts the blades at speeds around 100 m/s and imparts fatigue, resulting in the loss of material and accompanying aerodynamic losses and structural concerns [3,4]. The general literature on the aerodynamics of LEE [3–6] agrees on annual energy production (AEP) losses in the region of 0–3% (found both experimentally and numerically). Structural concerns relate to the erosion of the composite shell needing composite laminate repair which is difficult and costly to perform on an operational turbine. Leading edge protection (LEP) is therefore typically installed along the leading edge near the blade tip to mitigate or slow erosion. LEPs were traditionally tapes adopted from the aircraft industry, but the correct selection of an adhesive to achieve satisfactory installation whilst being able to contour the straight-sided tapes around the curved tips of blades has led to failure through delamination issues rather than erosion [7]. Currently, the use of coatings that can be

applied by a brush or roller [2], or pre-formed shells that are adhesively fixed to the blade surface, are more prevalent as commercial LEP products. No current LEP system lasts the lifetime of the turbine in an erosive environment onshore or offshore and so requires regular repair and replacement, sometimes in as little as one year. There is therefore high interest in the testing process used to test and certify improved LEP products being developed, as evidenced by WP4 in IEA Wind Task 46. The primary method for developing LEP systems and evaluating their rain erosion resistance is to perform rain erosion tests (RETs) using a whirling arm rain erosion test rig.

The R&D A/S whirling arm rain erosion tester, depicted in Figure 1, simulates the erosion of LEP materials on wind turbines by accelerating specimens through a rain field generated by 600 needles of the same droplet size [8]. The acceleration of the test compared to the wind turbine is generally created through increasing rotational speed and using higher than average rainfall intensities under a larger than average single droplet size. Typically, rotational speeds from 85 to 160 m/s are used under rainfall intensities from 26 to 34 mm/h with nominal 2.3–2.5 mm droplet sizes. These parameters are reflected in the high-speed (HALT) and low-speed (ALT) test requirements set by DNV-RP-0573 [9]. Note that, generally observed in practice, the only difference between HALT and ALT is rotational speed with the same rainfall intensity and droplet size being used for both tests. This range of combinations is specific to the R&D A/S test rig and will vary with other rotational arm test rig designs. There are 17 R&D A/S test rigs adopted by the wind industry at the time of writing, and it is the most common test rig design. The DNV-RP-0573 [9] details testing to be performed in DNV-RP-0171 [10], and the latter sets wind-sector-specific requirements of only using whirling arm rigs together with velocity–number (VN) curve analysis, above ASTM G73 [11]. An ISO standard for testing, ISO TS 19392-2 [12] is not currently used but is under revision to align with DNV-RP-0171 [10].

Figure 1. The R&D A/S whirling arm rain erosion tester at Offshore Renewable Energy (ORE) Catapult (Source: Offshore Renewable Energy Catapult).

When the whirling arm test was developed for the aerospace sector, the failure modes and order of failure for several different aerospace materials were assessed against failure observations on aircraft [13]. Similarly, for the wind sector, real turbine data were compared against rain erosion test performance as part of the COBRA working group [14]. However, the assessment did not cover the range of different LEP materials that are currently on the market for wind applications, with their wide range of mainly elastic to very viscoelastic properties. In addition, there has been a trend of increasing viscoelasticity over the last 5–10 years as these materials are observed to have better erosion performance. With the time- and strain-dependent response behaviour of viscoelastic materials [15–17], test parameters that affect these behaviours need to be re-evaluated to consider if the method

can accurately identify the order of performance of materials and accurately represent the realistic in-service behaviour. To assess the accuracy of the RET, first, the in situ environmental conditions must be well understood and then compared against recommended RET practices.

Precipitation data from ORE Catapult's National Offshore Anemometry Hub (NOAH) were examined by Herring et al. [18] to identify the characteristics of an offshore environment. Herring observed wide variation in precipitation intensity over a year with an average below 20 mm/h but spikes up to 126 mm/h with dry periods between. These trends align with the broader scientific literature [19,20]. Furthermore, studies on the effects of climate change [20,21] suggest rainfall intensities in extreme events versus various durations with different return periods are expected to increase by up to 17% by 2030, compounded by extreme monsoon seasons in global areas of offshore wind industry growth [22,23]. Herring [18] also illustrates the droplet size distributions (DSD) obtained according to Best's derived formulae adopted throughout the industry [24]. At NOAH, droplet sizes vary significantly, ranging from 0 to 3 mm. This variability is particularly pronounced during higher intensity rainfall events, which tend to produce larger droplets with greater impact energies, thereby increasing their erosive potential. These observations align with other research studies, where Letson and Pryor [19] estimated that the total kinetic energy of hydrometeor impacts can vary by up to 38% over four years, and Barfknecht [25] demonstrated that larger droplets are substantially more damaging than smaller ones, proposing an operational erosion-safe mode. Further studies [26–28] using finite element analysis (FEA) have all similarly emphasised the significant impact of droplet size on the stress field's size and shape during impact events, highlighting the critical role of droplet variability in assessing erosion. Conversely in testing, DNV-RP-0171 [10] uses a fixed droplet size of approximately 2 mm, which simplifies the testing process but overlooks these real-world dynamic effects and potentially underestimates the true erosive impact.

Researchers have also highlighted limitations in the reproducibility and control of current testing techniques, stressing the importance of defining a relevant and broad RET testing window for accelerated erosion testing. Caboni et al. [29] conducted rainfall measurements using disdrometers across offshore, coastal and onshore sites, correlating these data with erosion damage via the Palmgren–Miner rule. Their findings indicate that erosion is highly site-specific and significantly influenced by factors such as wind speed and rain rate. In one instance, 30% of annual erosion damage was predicted to have occurred within a 12 h period. Bech et al. [30] developed a droplet size-dependent model based on an expanded range of RETs with four droplet sizes between 0.76 mm and 3.5 mm. Compared to the recommended 2.38 mm singular droplet model, their new drop-size dependant model predicted a 2.35-fold increase in lifetime. Both studies underscore the impact of variance in environmental conditions on rain erosion resistance. In testing, DNV-RP-0573 [9] defines a narrow testing window, outlined in the first column of Table 1, with little to no variance in the parameters throughout testing. To fully determine whether these standard tests are adequate for evaluating LEP performance in real-world environments (outlined in the third column of Table 1), it is essential to first understand the isolated influence of the RET parameters.

To investigate a wider testing window more akin to in situ conditions, a two-phase testing campaign was established. DoE 1 performed the initial characterisation of each LEP and examined the influence of droplet impact frequency (variable 1 in Table 1) upon their rain erosion resistance, supported by DMA results. DoE 2 investigated the effects of droplet impact frequency sequencing, material recovery and droplet size (variables 2, 3, and 4 in Table 1, respectively) upon rain erosion resistance.

Table 1. RET experimental design space recommended by DNV-RP-0573 compared with in situ conditions.

Precipitation Variable	LEP Conditions Experienced in RETs According to DNV-RP-0573	LEP Conditions Experienced In Situ
1	The accelerated test (ALT) and highly accelerated test (HALT) use two distinct rotational speeds, 1200 rpm and 800 rpm, respectively, to drive two different droplet impact frequencies using constant single droplet size.	A broad range of intermittent droplet frequencies defined by the tip speed of the turbine.
2	A single droplet impact frequency is maintained consistently throughout the test duration.	Sequenced periods throughout the year of low-intensity events, followed by high-intensity events and vice versa.
3	Maintains a constant rain field with no interruptions.	Recovery periods throughout the year characterised by significant intervals of no rainfall.
4	A nominal droplet size of 2 mm is required, though in practice in R&D A/S rigs, the actual droplet size typically ranges between 2.3 and 2.5 mm.	A range of droplet sizes from 0.5 (below 0.5 mm expected not to impact) to 6 mm.

2. Materials and Methods

2.1. RET Procedure

ORE Catapult's R&D A/S whirling arm rain erosion tester was used to test two industrial LEP systems, which were quantitatively characterised using DMA following the protocols established by Jones et al. [17] described in Section 2.3 and Table 2. The rain erosion tester contains three rotational arms, each with a specimen holder, spinning horizontally with a range of speeds between 800 and 1200 rpm used for the tests. The water manifold, which is situated 400 mm above the rotating arm plane, consists of six hundred needles arranged at staggered intervals to ensure equal coverage of droplets over the LEP specimen whilst maximising falling velocity and minimising aerodynamic effects on the droplet trajectories. Three samples per test were evaluated for the DoE test campaigns described in Table 3 (DoE 1) and Table 5 (DoE 2). The samples were inspected for erosion damage regularly with the period between inspections set before the test started based on the expected length of the test. At each inspection period (slice), test engineers manually extracted the samples, removed any surface water and photographed them to document their condition using high-resolution cameras. Some selected tests were run in automated mode and the photographs from the internal rig camera were used. These data were validated against visual observations at the end of the test due to differences in image quality. Detailed records of the incubation locations and times for each sample were also maintained for cross-referencing against the images. The process was repeated sequentially until the erosion had penetrated through to the composite substrate on all three samples.

Both the DoE 1 and DoE 2 testing campaigns were conducted on two industrial LEP systems, LEP A and LEP B, which were selected based on their contrasting viscoelastic properties LEP A predominantly exhibited an elastic response under load, while LEP B demonstrated a substantially greater degree of viscoelastic behaviour.

LEP A is a system consisting of a filler and LEP and was applied to glass/epoxy RET samples sourced from Olsen Wings A/S. LEP B consists of a filler and LEP system which was applied over a specific blade-representative substrate. Products were applied to the test surfaces following the specific guidelines outlined in their respective technical datasheets. These application protocols included details on surface preparation. In both cases, the application was performed by a single individual using the same process for each sample

following best practice. All samples were cured for at least one week before testing and manufactured over the duration of the testing to minimise differences in curing times. No variations from different stages of curing were observed in the DoE test results.

2.2. RET Analysis

Using current analysis methods and DNV guidelines [9,10], there are two critical stages during a rain erosion test: the end of the incubation stage and sample failure otherwise known as a breakthrough. The end of the incubation stage is the point at which damage is first observed on the test specimen, defined by ASTM G73 [11] as a loss of material, surface deformation or any other changes in microstructure, properties or appearance. Sample failure, or breakthrough is the point at which the underlying substrate is exposed. Failure time is recorded conservatively as the time step preceding visible observation of the substrate. According to DNV-RP-0573 [9], fatigue data can be well described by a power law of type, where N is the specific number of impacts to failure, dependent on a variable associated with stress, in this case, impact velocity, V:

$$N = bV^{-m} \tag{1}$$

By representing as a log–log graph, the equation becomes a linear law allowing extraction of slope m and intercept b:

$$log(N) = log(b) - mlog(V) \tag{2}$$

Velocity is calculated from the erosion position on the specimen and rotational speed, while the specific number of impacts is calculated from the test time of incubation and the specific impact frequency. This specific droplet impact frequency is derived from a mathematical equation partially provided in [10] which accounts for the test rig geometry and testing conditions. It was used to generate the specific impact frequency values in Tables 3 and 5. However, not every part of the equation is well defined, e.g., the droplet falling velocity calculation, and it has been observed that different test houses use different calculations leading to a wide range of derived specific impact frequencies, so values used in this paper are specific to ORE Catapult's calculation.

Typically, a LEP with strong rain erosion performance would consistently incubate at higher velocities and sustain a greater number of impacts, resulting in a VN curve shifted toward the far right of the graph. This is illustrated in Figure 2, a synthetic example of a VN curve, where LEP Example 1 demonstrates superior performance compared to LEP Example 2. Figure 2 underscores the critical importance of larger datasets, as evidenced by the wider confidence band for LEP Example 1 compared to LEP Example 2, which is attributable to the smaller dataset available for LEP Example 1. The methodology used in this paper to compare VN curves for the differing tests works on the basis that a statistically significant deviation of the VN curve suggests that a targeted variable 1–4 in Table 1 is significant and should therefore be integrated into the test regimes.

The erosion damage progression rate, from incubation to breakthrough, depicted in Figure 3 is an additional novel method used to analyse the significance of the targeted variables in each DoE upon rain erosion resistance. It is assumed that a slower damage progression rate is desired in performance. The damage progression rate is calculated from the percentage difference between incubation and breakthrough times for each erosion point.

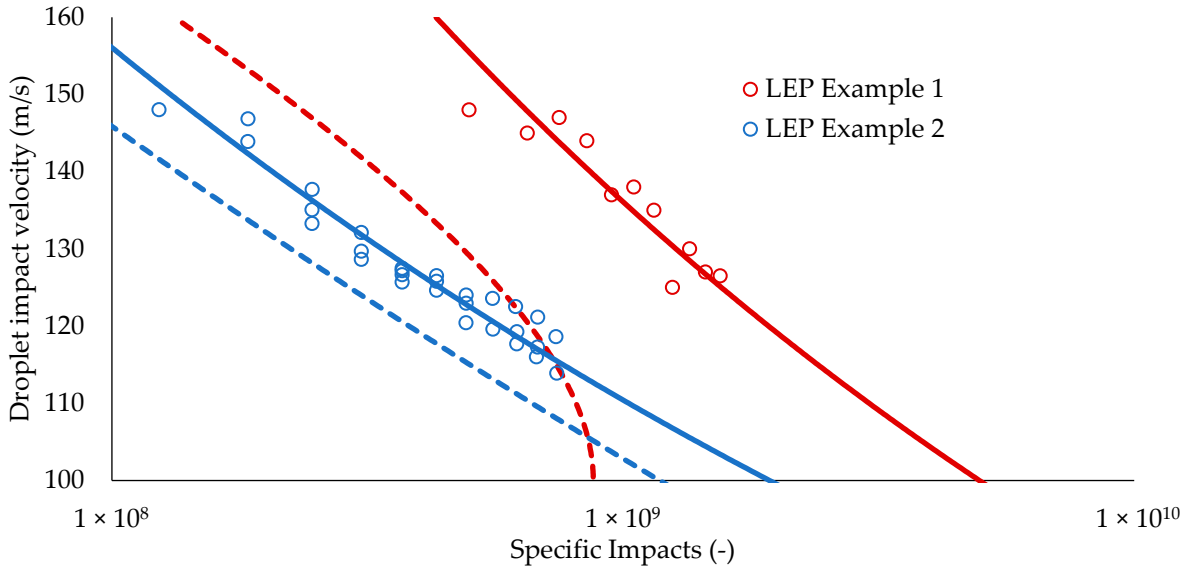

Figure 2. Example VN curve with two LEPs, LEP Example 1 and LEP Example 2 and their subsequent 50% and 95% confidence bands denoted with a solid and dotted line, respectively. These synthetic data are purely illustrative.

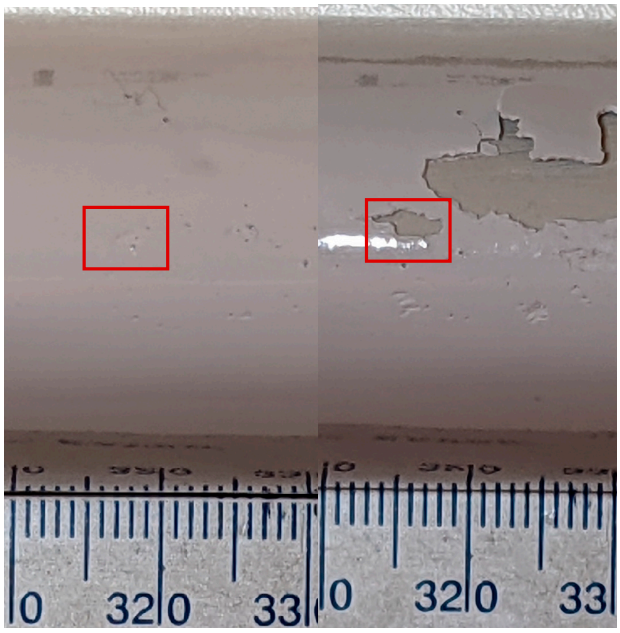

(**a**) (**b**)

Figure 3. Example damage progression behaviour from (**a**) incubation, followed by (**b**) breakthrough in later testing.

2.3. Dynamic Mechanical Analysis (DMA)

Film samples of LEP A and LEP B with approximate dimensions of 50 mm length × 10 mm width were obtained from cast LEP specimens using a freehand strip cutter (RDM Test Equipment, Stortford, UK). Dynamic mechanical analysis (DMA) was performed using a DMA 850 (TA Instruments, New Castle, DE, USA) with the modular tension clamp attachment. All DMA experimental procedures featured an initial conditioning step, and the temperature was equilibrated at the defined value for 5 min. Table 2 details the test parameters for all DMA performed in this study, which includes the use of several routine experimental procedures for the characterisation of viscoelastic materials in LEP applications, as previously reviewed [17].

Table 2. Test parameters for DMA oscillatory experimental procedures.

Experimental Procedure	Temperature (°C)	Amplitude (μm)	Frequency (Hz)
Oscillation strain sweep	20	0.1–10,000	1
Oscillation frequency sweep/time–temperature superposition (TTS)	−50 to 50 (at 10 °C intervals)	20	0.1–10 (per frequency sweep)
Oscillation fatigue test	20	20–500	1–200

Oscillation frequency sweep data acquired at 10 °C intervals between −50 and 50 °C and 0.1 to 10 Hz were used to extrapolate the values of E′, E″ and tan δ across a maximum frequency range of 10^{-2} to 10^{10} Hz by application of time–temperature superposition (TTS) within the TRIOS software package (v5.1.1) provided by TA Instruments. The validity of the produced TTS master curves was confirmed by shift factor analysis using the Williams–Landel–Ferry (WLF) and Arrhenius models within TRIOS, in accordance with the general method as detailed by Dorléans et al. [31]. The WLF model was exclusively used within the temperature region between the T_g and T_g + 100 °C to ensure the validity of the WLF equation [32]. Plots of the horizontal shift factors against temperature generated R^2 values > 0.99 in all cases, and the determined Arrhenius activation energy for each LEP (between 185 and 195 kJ/mol) was comparable with previous values obtained for other polymer classes used as LEP products [33].

3. RET DoE 1

3.1. Method

DoE 1 was used to characterise LEPs A and B in the widest possible range of droplet impact frequencies in the R&D A/S test rig using standard test procedures. Results were used to inform DoE 2. The rain erosion test parameters that influence droplet impact frequency were selected based on Pearson correlation tests to ensure no dependency between each parameter (correlation coefficients below 0.3) to avoid collinearity issues [34]. Such examples included rotational speeds, reflective of the range between the 800 rpm ALT and 1200 rpm HALT tests defined in DNV-RP-0573 [9], two needle sizes with various flow rates to cover the 0–3 mm droplet size range where pure droplet formation (not spraying) is created in the R&D A/S test rig at ORE Catapult and no inspection period under automated rig operation compared to 20 and 60 min removal for inspection to explore LEP recovery under non-rain periods. The outputted campaign is shown in Table 3.

Table 3. The testing campaign for DoE 1.

Test	Needle Size (G)	Rotational Velocity (rpm)	Flow Rate (L/h)	Inspection Period (mins)	LEP A		LEP B	
					Droplet Size (mm)	Droplet Impact Frequency (#/m^{2}s)	Droplet Size (mm)	Droplet Impact Frequency (#/m^{2}s)
T1	27	950	65	60	2.46	45,176	2.23	41,941
T2	22	1100	95	0	2.94	44,152	3.00	41,493
T3	27	1000	55	20	2.52	37,356	2.49	38,762
T4	22	1050	90	60	3.01	37,140	2.97	38,700
T5	22	900	95	0	2.94	36,125	3.00	33,949
T6	27	1200	35	20	2.55	27,505	2.55	27,505

3.2. Results and Discussion

Images from select test slices for T1 and T4 from one sample of each LEP, as illustrated in Figure 4, represent the general observations of the entire DoE 1. Visual inspection of these samples revealed that both LEP systems exhibited different failure modes at lower droplet impact frequencies (T3 to T6) compared to higher frequencies (T1 and T2). At lower droplet impact frequencies, each LEP exhibited a typical elastic failure or high-cycle fatigue failure mechanism. At higher droplet impact frequencies, each LEP exhibited a typical brittle or low-cycle fatigue failure mechanism. Table 4 outlines the qualitative criteria used to define these failure modes, which are based on extensive testing experience at ORE Catapult and the prior literature on viscoelastic failure mechanisms [35,36].

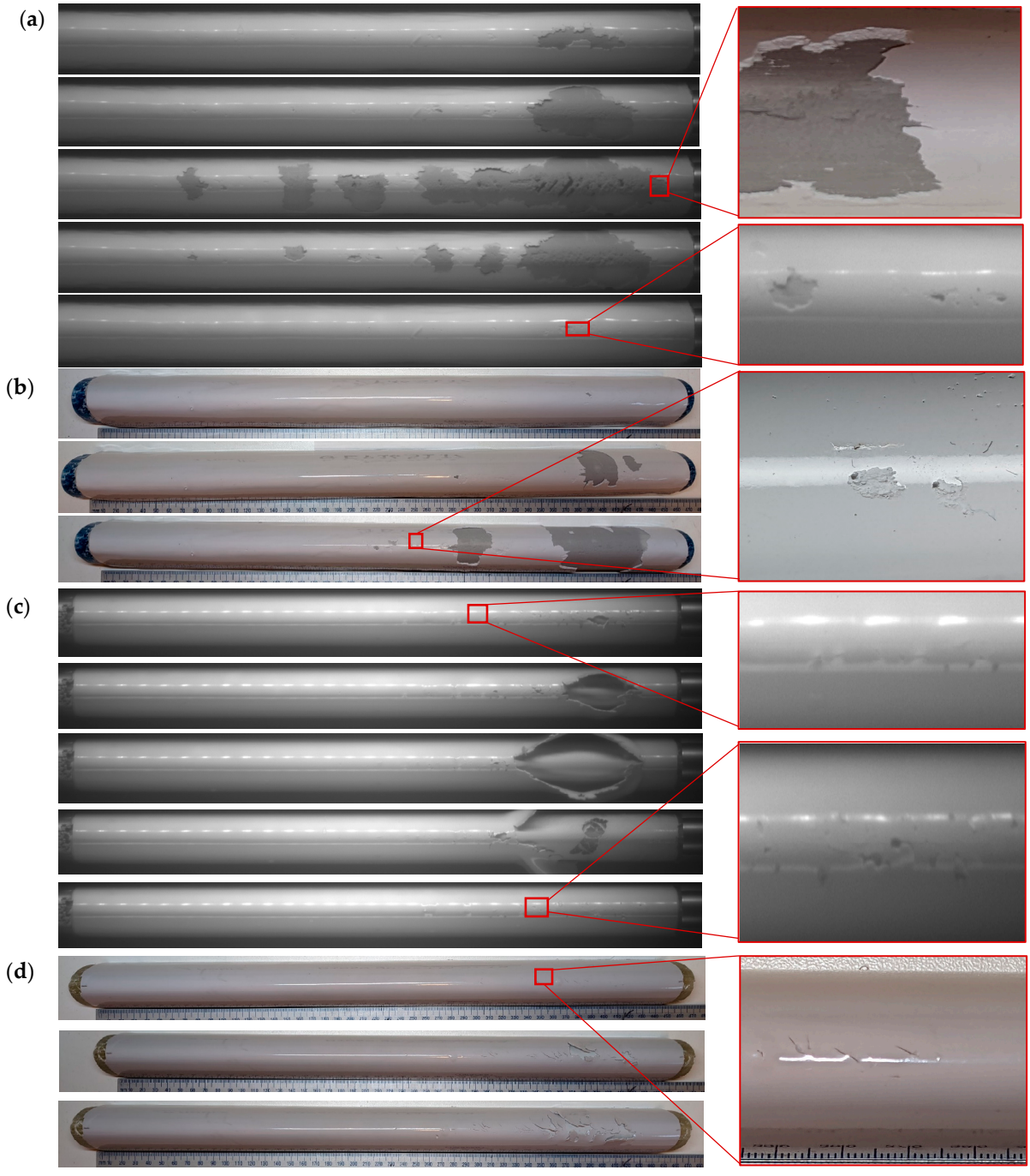

Figure 4. Representative images from selected test slices for T1 and T4, showing sample 1 for each coating. The high-velocity end of the test specimen is positioned on the right in all images. (**a**) LEP A

T1 Sample 1. Brittle fatigue mechanism—substantial number of damage sites that occur in correlation with linear velocity. Damage form has sharp edges with this becoming more apparent when chunks of material are removed; (**b**) LEP A T4 Sample 1. Elastic fatigue mechanism—damage occurs at distinct locations on the sample with no damage between sites. Damage sites have smooth edges; (**c**) LEP B T1 Sample 1. Brittle fatigue mechanism—substantial number of damage sites with cracking and tearing of LEP in multiple locations. Tearing progresses down the length of the sample; (**d**) LEP B T4 Sample 1. Elastic fatigue mechanism—small number of distinct damage sites consisting of cracks. Damage slowly progressed along the length of the sample.

Table 4. Criteria used to determine failure mechanism of LEP system.

Criteria	Elastic	Brittle
Number of damage sites	Few	Many
Relation of damage to the linear velocity	Minimal dependency (i.e., does not necessarily initiate at high-speed end of sample)	Highly dependent (i.e., initiates at high-speed end and propagates along the sample)
Relation to other damage	Damage is localised with no/minimal damage between local sites	Continuous damage along sample
Damage progression rate	Slow	Fast
Damage form	Smooth edges	Sharp edges

A summary of all testing performed in DoE 1 is provided in Figure 5, which illustrates the test length, droplet impact frequency and the determined failure mode for each test. LEP A exhibited a longer time to breakthrough in comparison to LEP B for tests T1 and T2 (at higher impact frequency tests), whereas the trend was reversed for T3 to T6, with LEP B exhibiting a longer time to breakthrough (at lower impact frequency tests). Note that the HALT test detailed in DNV-RP-0573 [9] has a similar specific impact frequency to T1 and T2 which sit above the elastic–brittle threshold observed for both LEPs A and B in Figure 5. It can be observed that performing HALT in isolation could reject LEP B instead of LEP A, whilst LEP B is significantly better performing in lower rotational speed tests.

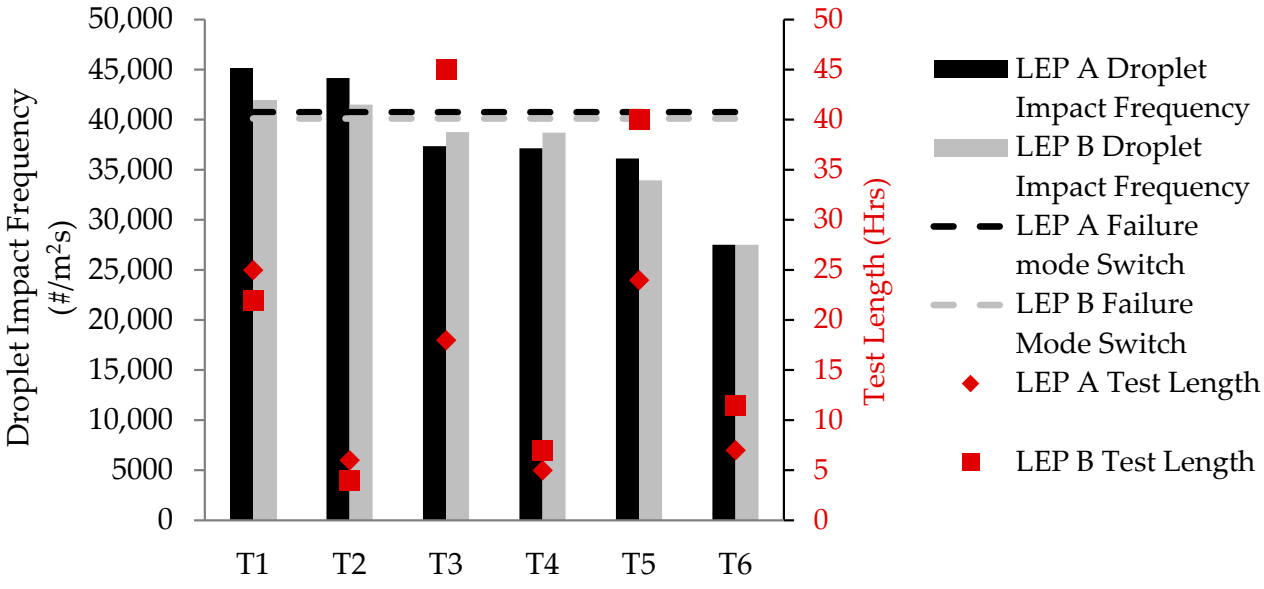

Figure 5. Summary of the test results including the droplet impact frequency for all tests in DoE 1, the discovered threshold between elastic and brittle failure, and the test lengths on the two LEP systems.

As observed in Figure 4, LEP A experienced pitting in accordance with typical damage mechanisms for LEP coating [35,36]. The LEP system exhibited poor interfacial adhesion between the LEP and the filler layers, which was evidenced by the delamination of large regions of LEP coating after a period of erosion damage. As defined in Table 4, the tests at higher impact frequencies (T1 and T2) introduced a large number of damage sites that developed at the high-speed end before propagating in correlation with the reduction in linear velocity along the length of the test specimen. The observed erosion damage features also contained sharp edges consistent with a brittle failure mechanism. At lower impact frequencies (T3 to T6), the damage did not always start at the high-speed end. Furthermore, the erosion damage features included smooth edges, which is consistent with an elastic failure mechanism. The failure mode changed based on the impact frequency, proving the hypothesis that the droplet impact frequency and, hence, the in situ precipitation intensity on a turbine change the failure mode of the LEP system. For LEP A, the determined droplet impact frequency threshold from high-cycle to low-cycle fatigue failure mechanisms is between 37,356 and 44,152 $m^{-2}s^{-1}$.

For samples of LEP B tested at a high impact frequency (T1 and T2), significant cracking was observed at the high-speed end of the test specimen with damage propagating quickly and joining to cause tearing of the LEP. In contrast, tests at lower impact frequencies (T3 to T6) exhibited a smaller number of cracks and tears at distinct points on the sample. The cracks showed minimal progression through the LEP material before failure occurred. For LEP B, the determined droplet impact frequency threshold from high- to low-cycle fatigue failure mechanisms is between 38,762 and 41,493 $m^{-2}s^{-1}$.

An explanation for the variation in rain erosion resistance with respect to test parameters for both LEP systems was explored further using DMA. Figure 6 illustrates E'' and tan δ values for LEP A and LEP B as a function of frequency upon the application of TTS to oscillation frequency sweep data. Previous studies [17] have inferred a correlation between increased values of E'' and tan δ and the rain erosion resistance of a material. The extrapolation of material properties at increased strain rates equivalent to those generated by the mechanism of droplet impact is also of particular interest (estimated to be 10^6 Hz [2]). It is observed that at frequencies < 100 Hz, LEP B exhibits higher E'' and tan δ values in comparison to LEP A. However, at frequencies > 100 Hz, LEP A exhibits higher E'' and tan δ values in comparison to LEP B. Although the reported strain rates generated by droplet impact are in the region of 10^6 Hz, it was deemed more applicable within this study to relate the values of E'' and tan δ at a measured test frequency within DMA to the specific impact frequency during a rain erosion test, i.e., a greater E'' and tan δ for LEP B at DMA test frequencies < 100 Hz may correlate to greater rain erosion resistance under high-cycle fatigue test conditions, and a greater E'' and tan δ for LEP A at DMA test frequencies > 100 Hz may correlate to greater rain erosion resistance under low-cycle fatigue test conditions.

Further DMA experiments were also performed to rationalise the superior performance of LEP A under low-cycle fatigue test conditions. The linear viscoelastic region (LVER) of a viscoelastic polymer material indicates the region at which the viscoelastic parameters are strain-independent below a critical strain. As illustrated in Figure 7, the critical strain corresponds to a 5% drop in the plateau storage modulus (E') value during an oscillation strain sweep. The critical strain values for LEP A and LEP B were calculated as 5.2 and 2.7%, respectively.

A series of oscillation fatigue experiments were also performed on LEP A and LEP B at amplitude values ranging between 20 and 500 μm, between frequencies of 1–200 Hz. A summary of the oscillation forces and stresses imparted upon both LEP materials during the oscillation fatigue experiments is presented in Figure 8, with each data point representing

the maximum oscillation stress and oscillation force imparted during each separate fatigue experiment. It is observed that LEP B undergoes irreversible plastic deformation outside of the LVER upon the application of oscillation forces above 3 N. However, no plastic deformation was observed for LEP A at imparted oscillation forces of up to 6 N. The oscillation strain sweep and oscillation fatigue experiments indicate that LEP B exhibits a lower critical strain value and is more prone to plastic deformation at relatively higher oscillation stresses. It is therefore reasonable to assume that LEP A may exhibit greater rain erosion resistance under test conditions that impart greater strain at increased frequency.

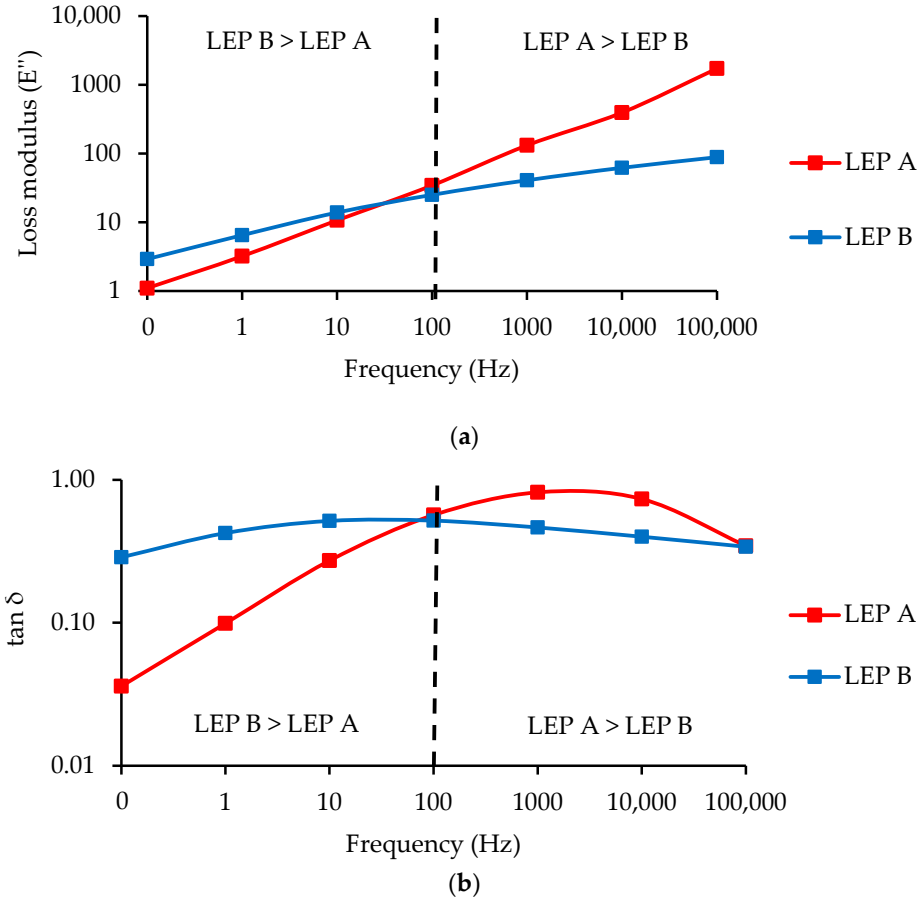

Figure 6. TTS master curves for E″ (**a**) and tan δ (**b**) as a function of frequency (Hz) at a reference temperature of 20 °C.

In conclusion, it is observed that there are qualitative correlations between the viscoelastic properties and the rain erosion resistance of LEP material as previously reviewed [17]. However, this study has demonstrated that there is also a requirement to consider the specific rain erosion test parameters when attempting to determine such material property–erosion correlations.

The results of DoE 1 highlight the critical need for understanding the effect of droplet impact frequency upon the rain erosion resistance of a LEP system. The observed transition from elastic to brittle failure at a threshold of approximately 40,000 $m^{-2}s^{-1}$ for the tested viscoelastic LEP systems indicates that testing at a single constant droplet impact frequency does not characterise the behaviour of a LEP sufficiently to produce a decisive order of failure for LEP comparison and selection. A DoE approach of at least 6 variations as used in Table 3 is recommended. There is also no guarantee that the DNV-defined HALT and ALT are going to represent the behaviour of the LEP and the range of real-world conditions it will be subjected to. Therefore, an improved understanding of droplet impact frequency

and failure mode during RET must be coupled with an understanding of droplet impact frequency and material response on the wind turbine blade in situ to fully validate the effectiveness of RET methods for all levels of viscoelasticity in LEPs.

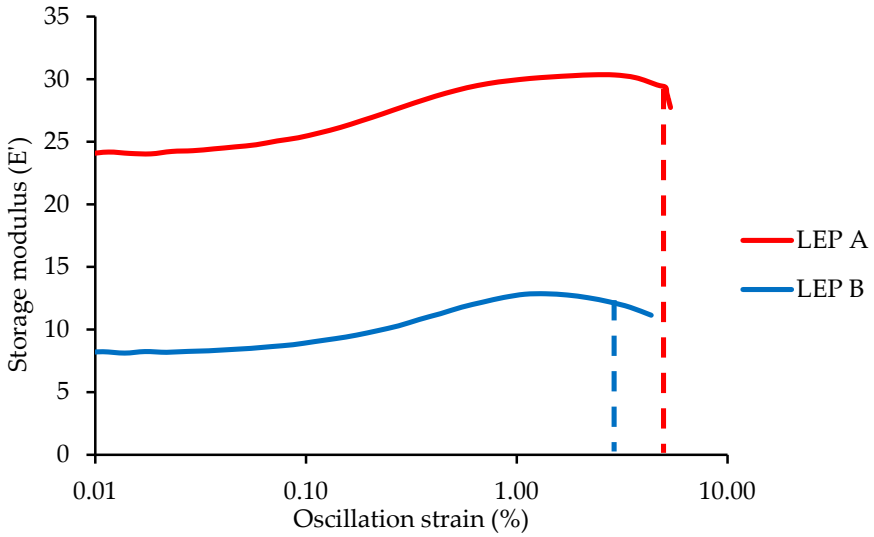

Figure 7. Oscillation strain sweep curves for LEP A and LEP B (20 °C, 1 Hz). The dashed line represents the end of the LVER or critical strain for each LEP.

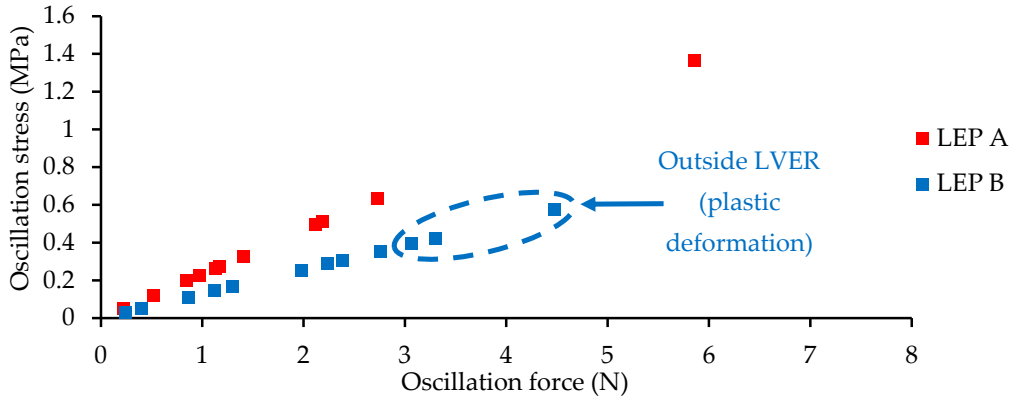

Figure 8. Summarised data from separate oscillation fatigue experiments conducted on LEP A and LEP B. Each data point represents the maximum imparted oscillation stress and oscillation force during each separate oscillation fatigue experiment.

4. RET DoE 2

4.1. Method

DoE 2 aimed to understand the influence of realistic rain parameters on the erosion process including sequencing of high- and low-cycle fatigue events, non-rain periods where recovery might occur and the stress variations in droplet size distributions compared to a single droplet size. These precipitation parameters are identified as variables 2, 3 and 4 in Table 1.

Different stress levels in a typical fatigue process cause different damage mechanisms to occur and interact. For composite materials, low-cycle fatigue is characterised by a brittle failure of the matrix through high-energy cracks that can penetrate rapidly across fibre bundles. In high-cycle fatigue, energy absorption mechanisms that slow damage progression such as fibre bridging and fibre pullout may occur. The switch in failure mode in DoE 1, with droplet impact frequency related to rotational speed and precipitation intensity, shows similarity to the composite fatigue process. It was surmised that the very

high precipitation intensities may act as low-cycle fatigue processes where embrittlement of the LEP occurs due to polymer chain freezing and lack of time for the viscoelastic portion of the loading curve to complete. In contrast, high-cycle fatigue processes would ensure the polymers remain more elastic as chains have time to flow and even recover through hydrogen bonding. T2 in DoE 1 evidenced this additional embrittlement with a high flow rate and larger droplet size. It was thought that a period of low-cycle fatigue (high precipitation intensity) at the start of the test may embrittle the LEP and lead to more rapid failure than if the low-cycle fatigue period happened later in the test sequence, so the effect was tested for confirmation.

The test conditions to impart low-cycle and high-cycle fatigue were determined based on the droplet impact frequency transitions of the LEP systems identified in DoE 1. Both LEP A and LEP B transitioned from high- to low-cycle fatigue at an impact frequency between 37,356 and 44,152 m^{-2} s^{-1} and between 38,762 and 41,493 m^{-2} s^{-1}, respectively. Therefore, high-cycle fatigue was determined with a droplet impact frequency below 37,356 m^{-2} s^{-1}, and low-cycle fatigue was determined with a droplet impact frequency above 44,152 m^{-2} s^{-1}. The rotational velocity is the most influential parameter in erosion performance, and this has been fixed between high-cycle and low-cycle with the impact frequency therefore changed through the flow rate alone. The following test conditions are used for each loading:

- High-cycle fatigue: 2.53 mm droplet size 1000 rpm, 45 L/h. Impact frequency = 32,017 m^{-2} s^{-1}.
- Low-cycle fatigue: 2.38 mm droplet size, 1000 rpm, 65 L/h. Impact frequency = 46,245 m^{-2} s^{-1}.

Based on the findings by Herring et al. that determined high-intensity events last for 11 min on average [18], the low-cycle fatigue test was 11 min in length. It is then assumed that a LEP might spend 10% of its time in low-cycle fatigue, making the high-cycle fatigue events 99 min in length. A rest period of 2 h was also included to examine if recovery after low-cycle fatigue would occur.

The effect of droplet size on rain erosion resistance has been previously documented [25,30]. The total stress effect is clearly non-linear with larger droplets being lower in number but significantly more damaging. This set of experiments will explore the validity of using the recommended droplet size of only 2 mm, by expanding testing to use G22, G27 and G32 needles in the test rig, corresponding to droplet sizes of 2.05, 2.40 and 2.95 mm, respectively. Each test uses a different single droplet size and results are analysed to explore statistical differences. The rotational velocity was held at 1000 rpm for all tests, whilst the flow rate was varied to ensure that the pressure in the water system was not exceeded and the droplets did not spray. Future research should investigate whether testing with a droplet distribution, similar to that observed in natural environments, is necessary and under what conditions it may be beneficial.

It is well known in polymer materials that, given time, the bonding interactions between chains may break, move and reform through secondary bonding mechanisms such as hydrogen bonding. This effect has also been observed in RETs comparing the removal of samples for inspection to automated running on the same LEP, with differences in time to failure of over 10 h. Currently, the length of the inspection period is not considered within RET procedures, and if tests are run in automated mode this may be a difference to in situ behaviour for lifetime predictions. Three tests of differing inspection periods and times between slices were selected: no inspection period, standard 1 h inspection period, and at least a 24 h inspection period. Table 5 summarises all the described tests that form DoE 2.

Table 5. The testing campaign for DoE 2.

Test	Motivation	Description	Test Conditions [RPM:Flow Rate (L/h):Droplet Size (mm)]
T1	Standard DNV-RP-0171 test (control)	Standard test with G27 needles and 1 h inspection period	1000:55:2.37
T2	Sequencing of high- and low-cycle fatigue loading as occurs in situ	Low-cycle fatigue–high-cycle fatigue–repeat	1000:45:2.53/1000:65:2.38
T3		High-cycle fatigue–low-cycle fatigue–repeat	1000:45:2.53/1000:65:2.38
T4		Low-cycle fatigue–rest period–high-cycle fatigue–repeat	1000:45:2.53/1000:65:2.38
T5	Exploration of the potential droplet size combination effect (uses T1)	Test with G32 needles	1000:30:2.05
T6		Test with G22 needles	1000:60:2.95
T7	Examination of the influence of the inspection period (uses T1)	No inspection period (test ran on automated mode)	1000:55:2.37
T8		At least 24 h inspection period	1000:55:2.37

4.2. Results and Discussion

4.2.1. Sequencing

The VN curves in Figure 9 illustrate the difference in rain erosion resistance of the different sequencing regimes. For both LEP systems, the high-cycle–low-cycle sequence resulted in the worst rain erosion performance, followed by the low-cycle–rest–high-cycle and then the low-cycle–high-cycle sequences, i.e., the opposite trend to what may be expected. Indicator–variable regression analysis was used to determine whether there was a statistical difference in VN curves [34,37]. A calculated *p*-value below 0.005 suggests that each different sequencing regime has a statistically significant impact on the VN curve and therefore the LEP performance. However, it was determined that additional VN data are necessary to achieve a more accurate curve fit. Subsequent R^2 values of 0.46, 0.47 and 0.60 for LEP A, and 0.60, 0.32 and 0.17 for LEP B, were calculated for the high–low, low–high, and low–rest–high curves, respectively. As a result, concrete conclusions cannot be drawn at this stage, and further testing is required.

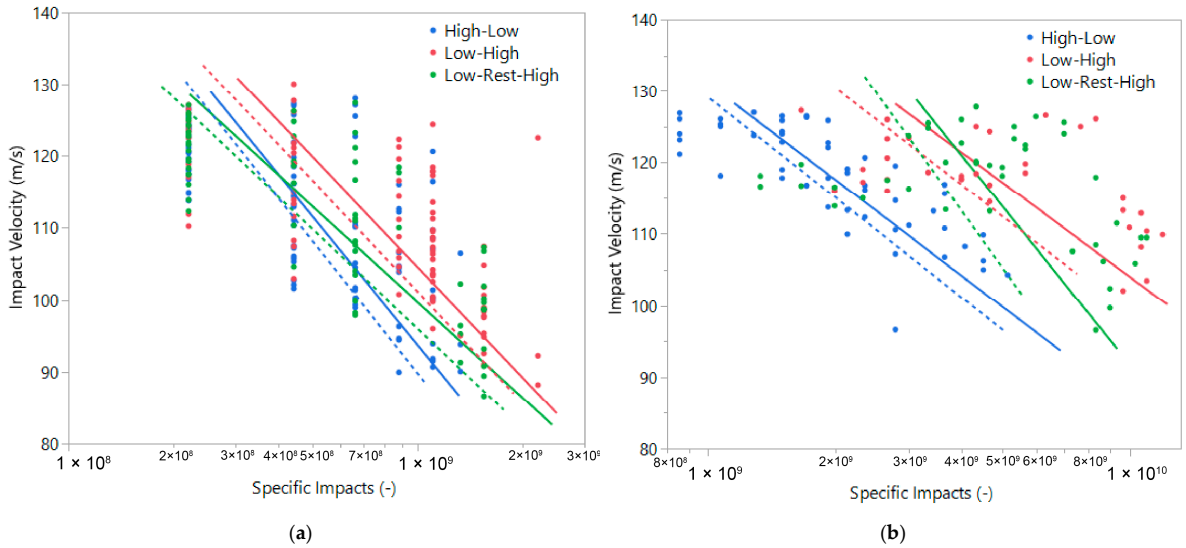

Figure 9. VN curves of erosion incubation on LEP A (**a**) and LEP B (**b**). Blue, red and green power fit and datapoints correspond to the high-cycle–low-cycle, low-cycle–high-cycle and low-cycle–rest–high-cycle fatigue sequences, respectively.

The performance metric of damage progression, as presented in Table 6, indicates an enhanced performance for the low-cycle–high-cycle sequencing in LEP A, evidenced by a slower damage progression rate. Conversely, LEP B did not exhibit a significant difference in the damage progression rate, which may be attributed to its tape composition, resulting in less consistent and more sporadic damage progression measurements.

Table 6. The percentage difference between the samples' time to incubation and time to breakthrough. This value corresponds to the damage progression rate through the material from incubation to the first sign of composite at breakthrough. Higher percentages suggest slower damage progression rates. Note: The CoV is based on the progression rate difference between the times to incubation and breakthrough and the original standard deviations of the three tested samples.

	LEP A		**LEP B**	
	% Difference from Incubation to Breakthrough	**CoV**	**% Difference from Incubation to Breakthrough**	**CoV**
T2: Low-cycle—High-cycle	700	33.1	444	22.7
T3: High-cycle—Low-cycle	367	24.8	445	24.0
T4: Low-cycle—Rest—High-cycle	533	9.1	562	18.8

4.2.2. Recovery

The VN curve analysis for differing recovery regimes, as depicted in Figure 10, suggests no observable difference in LEP performance with varying recovery times based on initial incubation points. Indicator–variable regression analysis for LEP A, with a *p*-value above 0.005, supports the conclusion that recovery times do not significantly impact LEP performance. For LEP B, despite a *p*-value below 0.005, the poor fit of the VN curve casts doubt on the reliability of this statistical outcome, highlighting challenges in applying RP VN curves to materials that deviate from a power law erosion pattern. Subsequent R^2 values of 0.60, 0.75 and 0.46 for LEP A, and 0.03, unavailable and 0.02 for LEP B, were calculated for the long inspection period, no inspection period and standard inspection period curves, respectively. This limitation underlines that VN curves focused only on incubation may not fully capture the effects of recovery periods on rain erosion resistance.

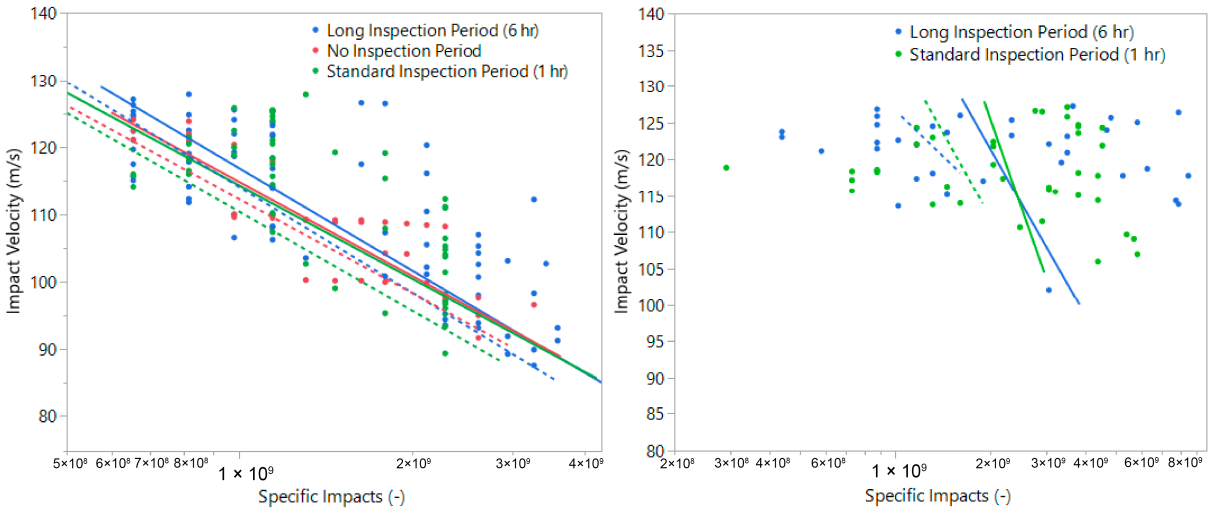

(**a**) (**b**)

Figure 10. VN curves of erosion incubation on LEP A (**a**) and LEP B (**b**). Blue, red and green power fit and datapoints correspond to the long, none and standard inspection periods, note for LEP B the no inspection period, automated camera test results were not of sufficient quality to analyse.

The damage progression rate data in Table 7 display contrasting results to the RET VN curve data, as longer inspection intervals (24 h or more) are associated with reduced damage progression rates compared to the standard 1 h inspection or no inspection intervals, which correlate with reduced performance in both LEP systems. These observations reinforce the notion that viscoelastic recovery in LEP materials, when given adequate time, can impact rain erosion resistance.

Table 7. The percentage difference between the samples time to incubation and time to breakthrough, full description on Table 6 caption.

	LEP A		LEP B	
	% **Difference from Incubation to Breakthrough**	**CoV**	% **Difference from Incubation to Breakthrough**	**CoV**
T7: Automated Inspection	300	88.6	172	22.0
T1: Standard Inspection (1 h)	875	55.0	506	69.6
T8: Long Inspection (at least 24 h)	1080	48.0	1100	37.2

4.2.3. Droplet Size

The VN curve analysis for differing droplet sizes of 2.95 mm, 2.37 mm and 2.05 mm, corresponding to needles G22, G27 and G32, respectively, as illustrated in Figure 11, reveals a marked decrease in LEP performance with larger droplets. Specifically, the 2.95 mm droplets result in a significant reduction in erosion resistance compared to the 2.37 mm and 2.05 mm droplets, which exhibit similar effects. Subsequent R^2 values of 0.52, 0.46 and 0.62 for LEP A, and 0.05, 0.02 and 0.31 for LEP B, were calculated for the G22, G27 and G32 curves, respectively, highlighting the need for more data or improved recommended practice on analysis to make concrete conclusions.

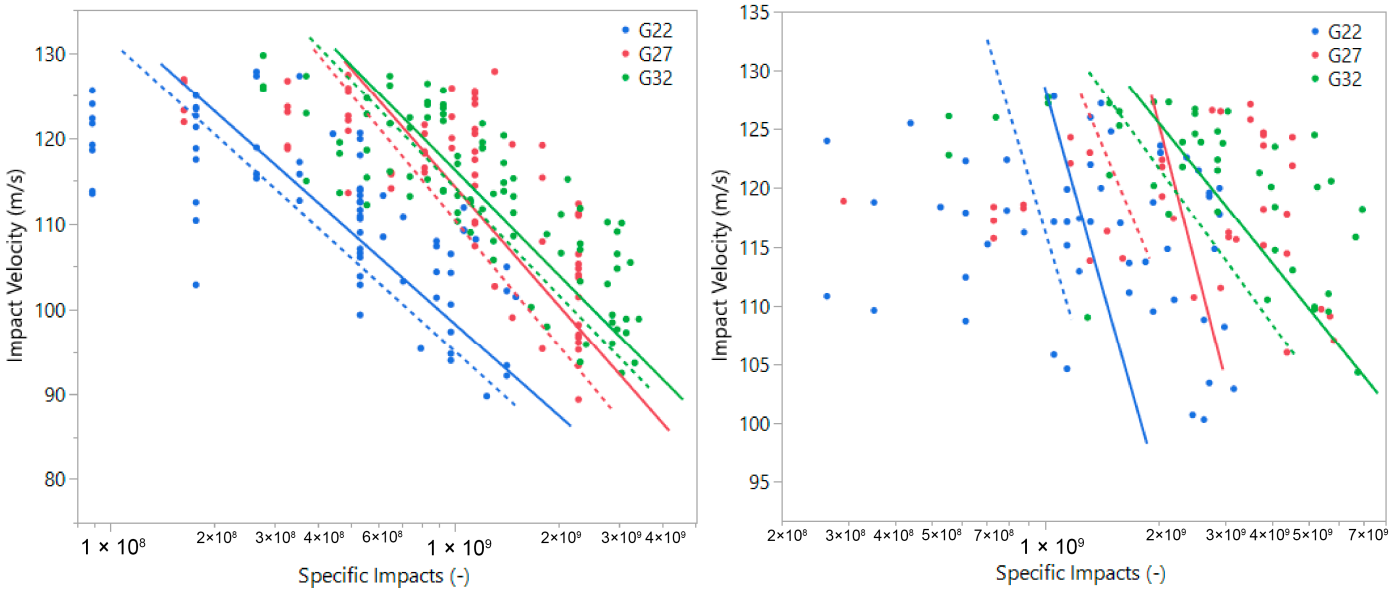

Figure 11. VN curves of erosion incubation on LEP A (**a**) and LEP B (**b**) with velocity denoting the position and specific no. impacts denoting the time. Blue, red and green power fit and datapoints correspond to the 2.95, 2.37 and 2.05 mm droplet sizes, respectively.

These findings align with the results published by Bech et al. [30], who conducted similar tests on four droplet sizes using the same DNV-RP-0171 [10] VN curve analysis. The agreement between these results supports the assertion that droplet size impacts LEP

performance. Consequently, the current RP of using a single nominal droplet size of 2 mm to characterise the erosion resistance of the material should be reconsidered and the range expanded for qualification.

Table 8, which outlines the damage progression rate for each droplet size tested in the RET, indicates no significant differences in the damage progression behaviour, suggesting that droplet size only affects the period to incubation for a LEP system.

Table 8. The percentage difference between the samples time to incubation and time to breakthrough, full description on Table 6 caption.

	LEP A		**LEP B**	
	% **Difference from Incubation to Breakthrough**	**CoV**	% **Difference from Incubation to Breakthrough**	**CoV**
T6: G22, 2.95 mm	1200	27.8	614	33.6
T1: G27, 2.37 mm	875	55.0	506	69.6
T5: G32, 2.05 mm	870	28.3	-	-

In practical scenarios, droplets impacting at any given time can vary widely in size, ranging from an estimated 0.5 mm to 6 mm. Therefore, future research should investigate the combined effects of different droplet sizes and the impact of small droplets (~0.5 mm) that cannot be tested in the current RET setup due to needle size limitations and test duration. This broader approach will provide a more comprehensive understanding of how various droplet sizes affect LEP performance.

5. Conclusions and Future Work

This study highlights the significant limitations of the current standard RET campaigns in accurately evaluating LEP systems for wind turbine blades. By comparing in situ precipitation conditions with the RET environments, it is evident that the simplistic parameters in current standards fail to replicate the complex erosive conditions experienced in real-world scenarios. Furthermore, the limitations of current testing methods stem from the recent advancements in LEP development towards viscoelastic materials, which show poor compatibility with the recommended analysis techniques. RET procedures have been developed in the aerospace industry where the materials used were typically elastic (e.g., metallics). Upon droplet impact, elastic materials respond instantaneously to the stress, and the response is completed before the next droplet impact. A viscoelastic material has the benefit of deforming under impact, dissipating the impact energy of the droplet, before recovering to its final configuration. However, this process is time-dependent and, if the time between impacts is short, the recovery of a LEP system from one droplet may interact with its deformation from the next impact. Due to the historic development of testing practices, this time-dependent behaviour is not factored into the current test method and standards.

The findings from the two-phase DoE approach underscore the importance of expanding the testing window to include a broader range of conditions defined in Table 1. Specifically, in DoE 1, a critical droplet impact frequency threshold for LEP A and B was identified, differentiating between elastic and brittle failure modes in viscoelastic LEP materials. This discovery suggests that standard tests, held at constant droplet impact frequencies throughout, may not provide a comprehensive assessment of LEP durability. The DoE 2 investigation into droplet impact frequency sequencing, recovery periods and varying droplet sizes, revealed that these factors also influence the performance and failure modes of LEP systems.

Building on these findings, future research should focus on the following key areas to improve the accuracy and reliability of LEP evaluations:

Representative testing campaign: This paper has highlighted the areas where current standards have limitations. Future work must convert this knowledge into a realistic testing campaign. This could extract environmental data from the desired environment and design a wide-window testing campaign that accurately evaluates a LEP.

More in situ LEP data: Field data give important insights into how a LEP performs in situ, compared to the RET. In closing this gap between testing and in situ performance, it is important to gather a vast amount of field data to verify methods.

Droplet impingement understanding: There is currently a gap in the literature on the droplet impact stresses for droplets impinging on a different wind turbine blade geometry to the RET specimen geometry; for example, large shear stresses caused by angled droplet impacts. Additionally, future work should investigate transitioning from the recommended specific droplet impact frequency metric to an impingement-based metric, which may offer an improved characterisation of droplet impacts.

Improved RET Analysis: The current subjectivity in RET analysis caused by ambiguous incubation definitions set by ASTM G73 [11] could be mitigated by incorporating automated processes. High-resolution imaging and automated analysis software could help minimise test engineer subjectivity and standardise practices across testing houses.

Author Contributions: Conceptualization, K.D., O.C. and P.S.; methodology, K.D.; funding acquisition, O.C., P.S.; software, P.K.; investigation, P.K., S.P. and S.J.; writing—original draft preparation, P.K.; writing—review and editing, K.D., O.C., S.P., P.S. and S.J.; supervision, K.D. All authors have read and agreed to the published version of the manuscript.

Funding: This research was funded by Carbo4power H2020-EU.2.1.3.—INDUSTRIAL LEADERSHIP—Leadership in enabling and industrial technologies—Advanced materials Programme (€7.8 million—Grant Agreement 953192) and industrial funding from GE Vernova and ORE Catapult.

Institutional Review Board Statement: Not applicable.

Informed Consent Statement: Not applicable.

Data Availability Statement: The datasets presented in this article are not readily available because of intellectual property restrictions. Requests to access the datasets should be directed to Peter Kinsley.

Conflicts of Interest: Authors O.C. and P.S. are employed by the company GE Vernova. The remaining authors declare that the research was conducted in the absence of any commercial or financial relationships that could be construed as a potential conflict of interest.

References

1. Keegan, M.; Nash, D.; Stack, M. On erosion issues associated with the leading edge of wind turbine blades. *J. Phys. D Appl. Phys.* **2013**, *46*, 383001. [CrossRef]
2. Herring, R.; Dyer, K.; Martin, F.; Ward, C. The increasing importance of leading edge erosion and a review of existing protection solutions. *Renew. Sustain. Energy Rev.* **2019**, *115*, 109382. [CrossRef]
3. Mendez, B.; Pires, O. Impact of high size distributued roughness elements on wind turbine performance. *J. Phys. Conf. Ser.* **2022**, *2265*, 032027. [CrossRef]
4. Gaudern, N. A practical study of the aerodynamic impact of wind turbine blade leading edge erosion. *J. Phys. Conf. Ser.* **2014**, *524*, 012031. [CrossRef]
5. Bak, C.; Guanna, M.; Olsen, A.; Kruse, E. What is the critical height of leading edge roughness for aerodynamics? *J. Phys. Conf. Ser.* **2022**, *2265*, 022023. [CrossRef]
6. Maniaci, D.; Westergaard, C.; Hsieh, A.; Paquette, J. Uncertainty Quantification of Leading Edge Erosion Impacts on Wind Turbine Performance. *J. Phys. Conf. Ser.* **2020**, *1618*, 052082. [CrossRef]

7. Maniaci, D.; MacDonald, H.; Paquette, J.; Clarke, R. *Leading Edge Erosion Classification System*; Sandia National Lab. (SNL-NM): Albuquerque, NM, USA, 2022.
8. Jensen-Johansen, N. *Test Methods for Evaluating Rain Erosion Performance of Wind Turbine Blade Leading Edge Protection Systems*; Technical University of Denmark: Kongens Lyngby, Denmark, 2020.
9. *DNV-RP-0573*; Evaluation of Erosion and Delamination for Leading Edge Protection Systems of Rotor Blades. DNVGL: Bærum, Norway, 2021.
10. *DNV-RP-0171*; Testing of Rotor Blade Erosion Protection Systems. DNVGL: Bærum, Norway, 2021.
11. *ASTM-G73*; Standard Test Method for Liquid Impingment Using Rotating Apparatus. ASTM: West Conshohocken, PA, USA, 2021.
12. *ISO/TS 19392-2*; Paints and Varnishes—Coating Systems for Wind-Turbine Rotor Blades—Part 2: Determination and Evaluation of Resistance to Rain Erosion Using Rotating Arm. ISO: Geneva, Switzerland, 2018.
13. Schmitt, G. *Flight Test-Whirling Arm Correlation of Rain Erosion Resistance of Materials*; AFML: Dayton, Ohio, USA, 1968.
14. Eisenberg, D.; Lausten, S.; Stege, J. Wind turbine blade coating leading edge erosion model: Development and validation. *Wind Energy* **2017**, *21*, 942–951. [CrossRef]
15. O'Carroll, A. Correlation of mechanical properties to rain erosion resistance of polymeric materials. Master's Thesis, University of Limerick, Limerick, Ireland, November 2018.
16. Imad, O.; Ward, C.; Hamerton, I.; Dyer, K. Engineering Viscoelastic Properties in Polyurethane Coatings to Reduce Erosion Risks in Wind Turbine Blades. *Sampe J.* **2021**, *57*, 16–24.
17. Jones, S.; Rehfield, N.; Schreiner, C.; Dyer, K. The Development of a Novel Thin Film Test Method to Evaluate the Rain Erosion Resistance of Polyaspartate-Based Leading Edge Protection Coatings. *Coatings* **2023**, *13*, 1849. [CrossRef]
18. Herring, R.; Dyer, K.; Howkins, P.; Ward, C. Characterisation of the offshore precipitation environment to help combat leading edge erosion of wind turbine blades. *Wind. Energy Sci.* **2020**, *5*, 1399–1409. [CrossRef]
19. Letson, F.; Pryor, S.C. From Hydrometeor Size Distribution Measurements to Projections of Wind Turbine Blade Leading-Edge Erosion. *Energies* **2023**, *16*, 3906. [CrossRef]
20. Martel, J.L.; Brisette, F.P.; Lucas-Picher, P.; Troin, M.; Arsenault, R. Climate Change and Rainfall Intensity-Duration-Frequency Curves: Overview of Science and Guidelines for Adaptation. *J. Hydrol. Eng.* **2021**, *26*, 03121001. [CrossRef]
21. Wang, X.; Huang, G.; Liu, J. Projected increases in intensity and frequency of rainfall extremes through a regional climate modelling approach. *J. Geophys. Res. Atmos.* **2014**, *119*, 13271–13286. [CrossRef]
22. *Global Offshore Wind Report*; World Forum Offshore Wind, Global Wind Energy Council: Brussels, Belgium, 2024.
23. Vinhoza, A.; Lucena, A.; Rochedo, P.; Schaeffer, R. Brazil's offshore wind cost potential and supply curve. *Sustain. Energy Technol. Assess.* **2023**, *57*, 103151. [CrossRef]
24. Best, A.C. The size distribution of raindrops. *Q. J. R. Meteorol. Soc.* **1950**, *76*, 16–36. [CrossRef]
25. Barfknecht, N.; von Terzi, D. Drop-size-dependent effects in leading edge rain erosion and their impact for erosion-safe mode operation. *Wind. Energy Sci.* **2024**. Available online: https://wes.copernicus.org/preprints/wes-2024-33/ (accessed on 12 November 2024).
26. Verma, A.S.; Castro, S.; Jiang, Z.; Teuwen, J. Numerical investigation of rain droplet impact on offshore wind turbine blades under different rainfall conditions: A parametric study. *Compos. Struct.* **2020**, *241*, 112096. [CrossRef]
27. Hoksbergen, T.; Akkerman, R.; Baran, I. Rain droplet impact stress analysis for leading edge protection coating systems for wind turbine blades. *Renew. Energy* **2023**, *218*, 119328. [CrossRef]
28. Tempelis, A.; Jespersen, K.; Dyer, K.; Clack, A.; Mishnaevsky, L. How leading edge roughness influences rain erosion of wind turbine blades? *Wear* **2024**, *552–553*, 205446. [CrossRef]
29. Caboni, M.; Slot, H.; Bergman, G.; Wouters, D.; Van der Mijle Meijer, H. Evaluation of wind turbine blades' rain-induced leading edge erosion using rainfall measurements at offshore, coastal and onshore locations in the Netherlands. *J. Phys. Conf. Ser.* **2024**, *2767*, 062003. [CrossRef]
30. Bech, J.; Jensen-Johansen, N.; Madsen, M.; Hannesdottir, A.; Hasager, C. Experimental Study on the Effect of Drop Size in Rain Erosion Test and on Lifetime Prediction of Wind Turbine Blades. *Renew. Energy* **2022**, *197*, 776–789. [CrossRef]
31. Dorleans, V.; Delille, R.; Notta-Cuvier, D.; Lauro, F.; Michau, E. Time-temperature superposition in viscoelasticity and viscoplasticity for thermoplastics. *Polym. Test.* **2021**, *101*, 107287. [CrossRef]
32. Ljubic, D.; Stamenovic, M.; Smithson, C.; Nujkic, M.; Medo, B.; Putic, S. Time-temperature superposition principle—Application of WLF equation in polymer analysis and composites. *Zast. Mater.* **2014**, *55*, 395–400. [CrossRef]
33. Ouachan, I. Characterisation and Understanding of Viscoelastic Leading Edge Protection Solutions Used on Offshore Wind Turbines. Ph.D. Thesis, University of Bristol, Bristol, UK, 2022.
34. Schober, P.; Schwarte, L. Correlation Coefficients: Appropriate Use and Interpretation. *Anesth. Analg.* **2018**, *126*, 1763–1768. [CrossRef] [PubMed]

35. Ansari, Q.; Sanchez, F.; Domenech-Ballester, L.; Young, T. Evaluation of Offshore Wind Turbine Leading-Edge Protection Coating Failure Mode under Rain Erosion. *Procedia Struct. Integr.* **2024**, *52*, 122–132. [CrossRef]
36. Katsivalis, I.; Chanteli, A.; Finnegan, W.; Young, T. Mechanical and interfacial characterisation of leading-edge protection materials for wind turbine blade applications. *Wind. Energy* **2022**, *25*, 1758–1774. [CrossRef]
37. Miller, J.; Erickson, M. On Dummy Variable Regression Analysis. *Sociol. Methods Res.* **1974**, *2*, 409–430. [CrossRef]

Disclaimer/Publisher's Note: The statements, opinions and data contained in all publications are solely those of the individual author(s) and contributor(s) and not of MDPI and/or the editor(s). MDPI and/or the editor(s) disclaim responsibility for any injury to people or property resulting from any ideas, methods, instructions or products referred to in the content.